Journal of Materials Chemistry A

Accepted Manuscript

This article can be cited before page numbers have been issued, to do this please use: Y. Xu, S. Wang, J. Yang, B. Han, R. Nie, J. Wang, Y. Dong, X. Yu, J. Wang and H. Jing, *J. Mater. Chem. A*, 2018, DOI: 10.1039/C8TA03315C.

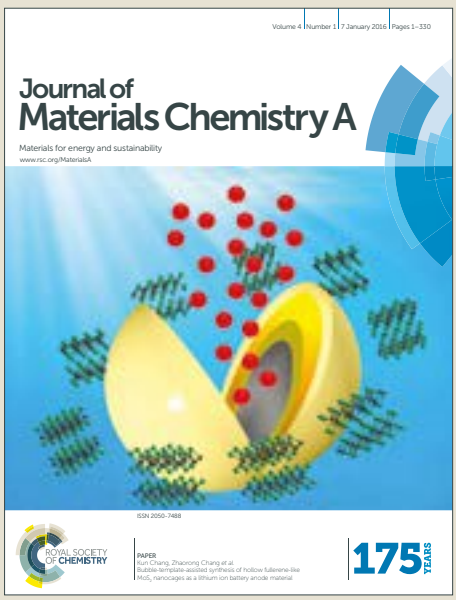

ROYAL SOCIETY OF CHEMISTRY

rsc.li/materials-a

View Article Online
DOI: 10.1039/C8TA03315C

Journal Name

ARTICLE

Highly efficient photoelectrocatalytic reduction of CO_2 on the Ti_3C_2/g-C_3N_4 heterojunction with rich Ti^{3+} and pyri-N species

Received 00th January 20xx,
Accepted 00th January 20xx

DOI: 10.1039/x0xx00000x

www.rsc.org/

Yanjie Xu,[a] Shuai Wang,[b] Jun Yang,*[b] Bo Han,[a] Rong Nie,[a] Jixian Wang,[a] Yapeng Dong,[a] Xiaogang Yu,[a] Jianguo Wang[c] and Huanwang Jing*[a,c]

The photoelectrocatalytic (PEC) reduction of CO_2 into chemical fuels in water is conceived as a promising route to mitigate energy crisis and global warming issues. Herein, Ti_3C_2/g-C_3N_4 (TCCN) heterojunctions were fabricated by in-situ heating treatment and applied to PEC CO_2reduction. These heterojunctions have narrow band gaps (2.3-2.6 eV) and rich Ti^{3+} species, which are beneficial to the absorption of solar light and the separation of electrons and holes. Besides, the abundant pyri-N species in TCCN heterojunctions could adsorb CO_2 molecules, which is favourable for the CO_2 reduction. The deposition of nanometal particles would accelerate the charge transfer obviously. In the two-electrode system of M-TCCN||$BiVO_4$, the total formation rate of formate and methanol can be as high as 50.2 $\mu Mcm^{-2}h^{-1}$ (25.1 $mMh^{-1}g^{-1}$) that is tenfold than that of pristine g-C_3N_4. The carbon source of products was verified by $^{13}CO_2$ labeling experiment. These heterojunctions show outstanding PEC performance and stability, which can be used as promising candidates in solar-to-fuel engineering field.

1. Introduction

The renewable energy, such as sunlight, wind and geothermal heat, is a viable substitute for fossil fuels. Converting CO_2 into chemical fuels using solar energy is considered as a sustainable avenue to alleviate energy crisis and global warming issues in the future.[1-5] In the natural photosynthesis system, green plants convert CO_2 and H_2O into hydrocarbons under the irradiation of sunlight, which suggests that the CO_2 might be transformed into chemical fuels by imitating the natural photosynthesis.[6-8] The photocatalysis and PEC reduction of CO_2 are attractive approaches to convert solar energy into renewable chemical fuels.[9-15] Particularly, the PEC method is more efficient than photocatalysis because that the external voltage could accelerate the transfer of charge carries and suppress the recombination of photo-generated electron-hole pairs.[16-19] Therefore, it is feasible to construct PEC system to generate chemical fuels by achieving the coupling of water splitting and CO_2 reduction.

Graphitic C_3N_4 (g-C_3N_4) has been proved to be a fascinating semiconductor for photocatalysis since it is facile synthesized, earth-abundant and physicochemically stable.[20-25] However, bulk g-C_3N_4 always suffers from low electrical conductivity, low surface area and high recombination rate of charge carriers, which confines its applications in photocatalysis.[26-29] In order to obtain efficient g-C_3N_4-based photocatalysts for solar fuel conversion, many strategies have been developed, for example, depositing metal nanoparticles and forming heterojunction with other semiconductor.[30-38]

Ti_3C_2, a layered two-dimensional (2D) transition metal carbide belonging to MXenes, possesses excellent hydrophily, structural stability, high electrical conductivity and superior light-harvesting ability.[39-44] Nevertheless, there are few reports about the applications of MXenes in the renewable energy conversion so far.[45, 46] Presumably, combining g-C_3N_4 and Ti_3C_2 to form heterojunction might be an effective strategy to fabricate an efficient photocatalyst, which may exhibit strong ability of light absorption and high efficiency of charge separation in CO_2 reduction reaction.

In this work, a series of Ti_3C_2/g-C_3N_4 heterojunctions were prepared by a facile heating method and used as photocathodes in the CO_2 PEC reduction experiments. It is confirmed that these new TCCN heterojunctions have narrow band gaps, rich Ti^{3+} and pyri-N species, which are favourable for the CO_2 reduction. Besides, a possible mechanism was carefully proposed.

2. Experimental

2.1 Preparation of Ti_3C_2 sheets

Commercially available powders of Ti, Al and graphite were used as raw materials to synthesize Ti_3AlC_2 powder. The detailed synthesis method can be found elsewhere.[47,48] Then 2D Ti_3C_2 sheets were

[a] State Key Laboratory of Applied Organic Chemistry, College of Chemistry and Chemical Engineering, Lanzhou University, Lanzhou 730000, P. R. China. *E-mail: hwjing@lzu.edu.cn; Fax: 86-931-8912582. Tel: 86-931-8912585.
[b] State Key Laboratory of Solid Lubrication, Lanzhou Institute of Chemical Physics, Chinese Academy of Sciences, Lanzhou 730000, P. R. China. *E-mail: jyang@lzb.ac.cn.
[c] State Key Laboratory of Coal Conversion, Institute of Coal Chemistry, Chinese Academy of Sciences, Taiyuan 030001, P. R. China.
Electronic Supplementary Information (ESI) available See DOI: 10.1039/x0xx00000x

View Article Online
DOI: 10.1039/C8TA02315C

fabricated by selectively exfoliating the Al atoms from Ti_3AlC_2 powders in aqueous HF solutions (40 %) for 24 h at room temperature. The obtained Ti_3C_2 specimens were rinsed repeatedly with deionized water to neutral and dried in vacuum.[48]

2.2 Preparation of Ti_3C_2/g-C_3N_4 (TCCN) heterojunctions

The TCCN heterojunctions were prepared by a feasible in-situ heating treatment method. Briefly, 15 g thiourea with different mass contents of Ti_3C_2 (50:1, 20:1 and 10:1) was mixed and ground in an agate mortar for 30 min to obtain homo-disperse mixture. Subsequently, the mixture was placed into a crucible that was wrapped tightly with aluminium foil, and then annealed at 500 °C for 2 h in muffle furnace. The obtained samples were designated as TCCN1 (50:1), TCCN2 (20:1), TCCN3 (10:1), respectively. The pristine g-C_3N_4 was also prepared by the same method using thiourea as raw material and labelled as CN.

2.3 Preparation of CN/FTO and M-TCCN/FTO electrodes

The TCCN heterojunctions were deposited onto clean FTO glasses by an electrophoretic deposition method.[44] A typical procedure was described as follows: 50 mg different samples and 10 mg iodine were dispersed into 50 mL acetone; then the particles were deposited onto the FTO glass under 20 voltage provided by a DC power supply for 15 min; lastly, the metal (M = Pd, Pt, Au) nanoparticles (NPs) were deposited by electrodeposition to gain M-TCCN/FTO electrodes according to our previous report.[19]

2.4 Photoelectrochemical measurement and CO_2 reduction experiments

The photoelectrochemical properties of photocathodes were characterized by an electrochemical workstation (CHI660E). The M-TCCN/FTO, $BiVO_4$/FTO and Ag/AgCl were employed as working electrode, counter electrode and reference electrode, respectively in a tri-electrode system of M-TCCN|Ag/AgCl|$BiVO_4$. The electrochemical impedance spectroscopy (EIS) and the Mott-Schottky plots were collected under the dark condition in the tri-electrode system. The linear sweep voltammetry (LSV) curves and the amperometric photocurrent responses were detected in the two-electrode system of M-TCCN||$BiVO_4$.

The PEC reduction of CO_2 experiments were performed with the two-electrode system of M-TCCN||$BiVO_4$ in the electrolyte of $KHCO_3$ aqueous solution (0.1 M, pH = 6.8, 50 mL). The external voltages (–0.45 V, –0.65 V, –0.85 V and –1.05 V) were powered by a Silicon solar cell. The light intensity was 200 mW/cm^2 and provided by a 300 W Xenon lamp (PLS-SXE300/300UV). The liquid products were identified by ^{1}H NMR (JNM-ECS 400 MHz) spectra with water suppression, using DMSO (10 mM) and *m*-trihydroxybenzene (MTB, 50 mM) as internal standards.[19] The gas-phase products were determined by gas chromatography (GC, CP-3380 Varian).

2.5 Morphology and structure characterization

The phase constituents of as-prepared specimens were identified by XRD (D/max-2400 Rigaku) with Cu Kα radiation. The morphologies of CN and TCCN samples were observed by field emission scanning electron microscope (FESEM, JSM-6701F) and field emission transmission electron microscope (TEM, Tecnai G2 TF30). The elements chemical states of specimens were identified by XPS spectra on a Kratos AXIS Nova spectrometer (Shimazu Co., Ltd.). The UV-vis absorption spectra were collected on a UV-vis spectrophotometer (UV-2600, Shimadzu). The electron paramagnetic resonance (EPR) spectra were recorded by a Bruker ER200DSRC10/12 spectrometer at room temperature. The photoluminescence (PL) emission spectra were recorded on a FLS920 spectrofluorometer with an excitation wavelength of 325 nm. The N_2 adsorption-desorption and the CO_2 sorption isotherms were measured at −196 °C and 25°C, respectively, using a micrometrics sorption analyzer (TriStar II 3020). The CO_2 temperature programmed desorption (TPD) was conducted on a TP-5080 catalyst characterization instrument with a TCD detector. Prior to the measurement, the samples were heated at 300 °C for 1 h in helium gas environment.

3. Results and discussion

3.1 Characterization of photocatalysts and photocathodes

The XRD patterns of photocatalysts are displayed in Fig. 1a. It can be clearly seen that the XRD pattern of TCCN3 has two distinct feature peaks around 13.0° and 27.4°, which correspond to the (100) and (002) planes of g-C_3N_4, respcectively.[21] The (002), (004) and (110) planes of Ti_3C_2 are appeared and labelled in Fig. 1a, as well.[49] With the increasing Ti_3C_2 content, the diffraction signals of g-C_3N_4 nanosheets weaken evidently, while the signals of Ti_3C_2 strengthen gradually. As shown in Fig. 1b, the shoulder peak at 25.3° corresponds to the (101) plane of anatase TiO_2,[19, 50] revealing that small amounts of TiO_2 was formed during the fabrication processes of TCCN samples.

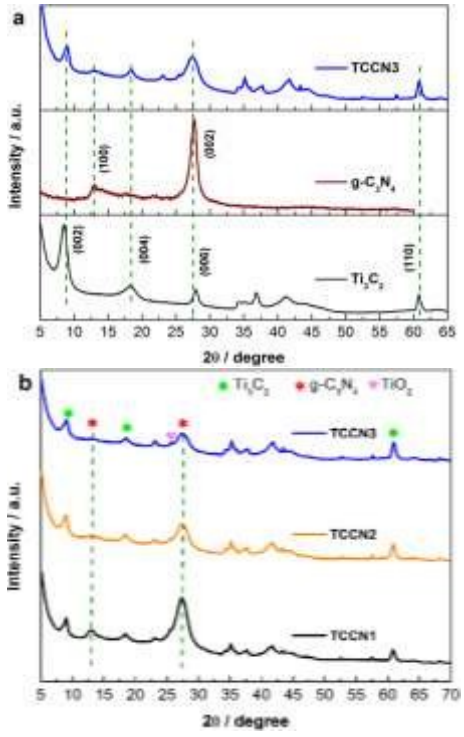

Fig. 1. XRD patterns of (a) g-C_3N_4, Ti_3C_2 and TCCN3, and (b) different TCCN samples

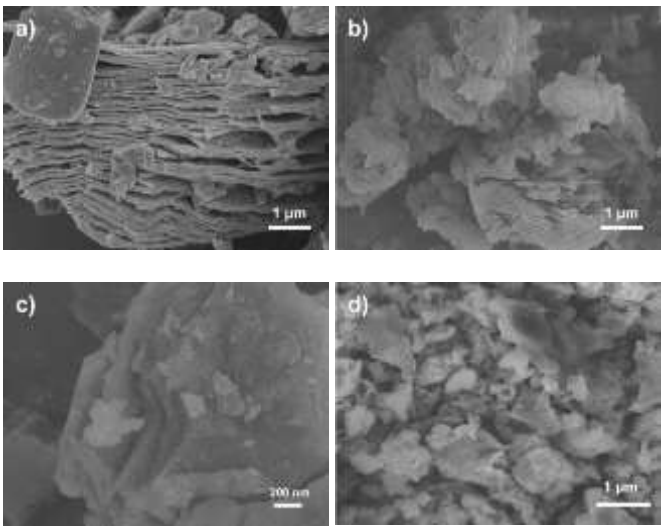

Fig. 2. FESEM images of (a) Ti_3C_2, (b) g-C_3N_4, (c) TCCN and (d) TCCN-FTO samples

As shown in Fig.2, the as-prepared Ti_3C_2 sheets (Fig. 2a) has a more obviously laminate structure than the pristine g-C_3N_4 (Fig. 2b). It can be seen from Fig. 2c that the TCCN shows a partially-covered layered structure, indicating that g-C_3N_4 is successfully decorated on the Ti_3C_2 sheets surface. As shown in Fig. 2d, the TCCN samples still retain the covered layered structure after electro-depositing onto the FTO glasses, and the thickness of TCCN film is about 6 μm (Fig. S1).

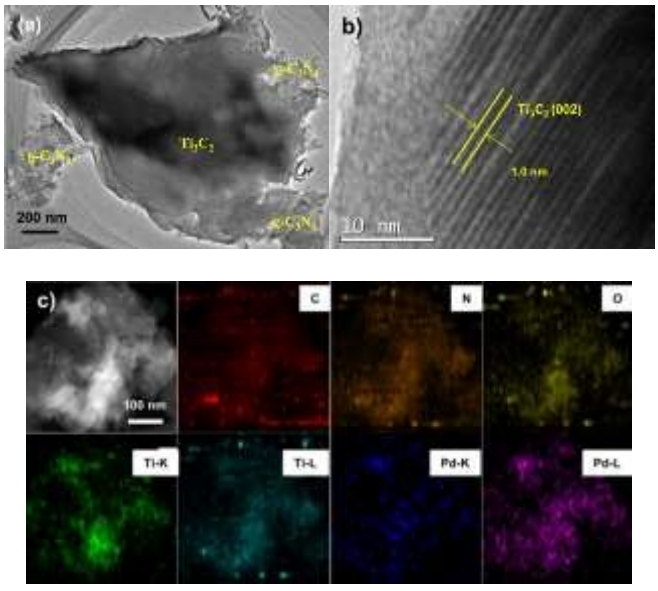

Fig. 3. (a,b) TEM images and (c) EDS mappings of Pd-TCCN3

TEM images of the Pd-TCCN photocathode are displayed in Fig. 3 and Fig. S2. It clearly illustrates a heterojunction interface between the g-C_3N_4 and Ti_3C_2 phases. The high magnification TEM image demonstrates the diffraction plane (002) of Ti_3C_2 phase (Fig. 3b).[45] Notably, the EDS mappings reveal that the C, N, O, Ti and Pd elements are well distributed onto the surfaces of Pd-TCCN electrode, validating that the heterojunctions were formed.

Fig. 4 and S3 demonstrate the XPS spectra of photocathodes. According to the survey spectrum of TCCN3, the binding energy peaks of Ti element are appeared in comparison with that of pristine g-C_3N_4, indicating that the Ti_3C_2 species are incorporated into the g-C_3N_4 phase (Fig. 4a). As shown in the high resolution spectrum of Ti 2p, the binding energies at 454.8 and 460.3 eV, 458.2 and 463.7 eV are assigned to Ti−C and Ti−O species, respectively (Fig. S3).[45] For the C 1s spectrum of TCCN3, the peak at 286.0 eV corresponds to C−OH due to the join of Ti_3C_2.[36,51] Furthermore, the high resolution XPS spectra of N 1s in TCCN3 and CN were analyzed detailedly. The binding energies at 398.5 eV, 399.5 eV and 400.8 eV are assigned to the C−N−C (pyri-N), N−$(C)_3$ and N−H groups, respectively (Fig. 4b).[52-54] When the TCCN3 heterojunction was formed, in comparison with CN, the concentration of pyri-N increased from 45.2 % to 57.2 %. The presence of abundant pyri-N species in the TCCN could facilitate the adsorption of CO_2,[51-53] and enhance the activity of CO_2 reduction consequently.

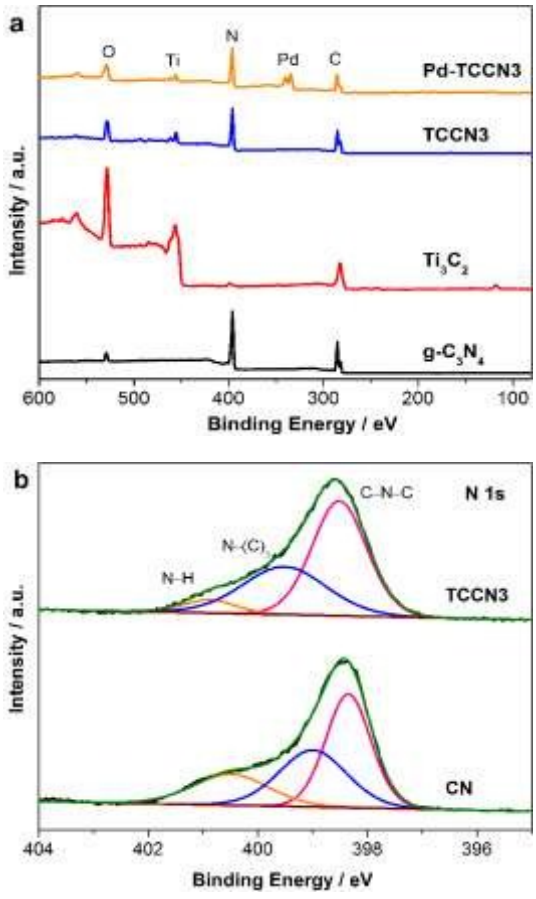

Fig. 4. (a) XPS survey spectra of g-C_3N_4, TCCN3 and Pd-TCCN3 electrodes, (b) high resolution XPS spectra of N 1s in CN and TCCN3

Moreover, after depositing the metal NPs onto the TCCN3 electrodes, the binding energy of Pd, Au and Pt were measured. As shown in Fig. S3, the peaks at 342.9 and 337.6 eV are assigned to 3d orbital of Pd,[55] peaks at 83.3 and 87.0 eV are belonged to 4f orbital of Au, and peaks at 75.4 and 72.2 eV are attributed to 4f orbital of Pt. The above results reveal that the metals NPs were deposited on

the surface of electrode, and the target M-TCCN electrodes were fabricated successfully.

In the EPR spectra (Fig. 5a), the pristine g-C_3N_4 shows a weak signal with Landé factor (*g*) of 2.004, which is derived from the unpaired electrons on the aromatic rings.[20] Obviously, there are two strong signals with g = 2.004 and g = 1.94 for TCCN heterojunctions, and the intensities of signals are gradually enhanced with the increase of Ti_3C_2 content. It was reported that the signal at g = 1.94 is assigned to the Ti^{3+} species that could provide trapping centres for charge carriers and suppress the recombination of photogenerated electrons and holes.[56-59]

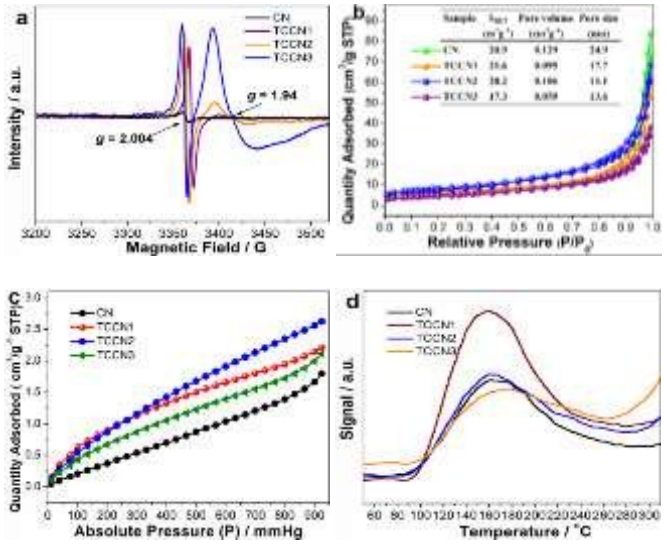

Fig. 5. (a) EPR spectra measured at room temperature, (b) N_2 adsorption-desorption isotherms measured at −196 °C, (c) CO_2 adsorption isotherms measured at 25 °C and (d) CO_2 TPD profiles of different samples

As shown in the Fig. 5b, the N_2 adsorption–desorption isotherms reveal that the surface areas of TCCN are enlarged gradually as Ti_3C_2 content increased. The TCCN2 sample possesses the largest surface area of 28.2 m^2 g^{-1}, while the TCCN3 has the smallest surface area of 17.3 m^2 g^{-1}, because the pure Ti_3C_2 has a relatively small surface area.[60] Moreover, their pore sizes of mesoporous are gradually narrowed from CN to TCCN3 sample.

The CO_2 sorption experiments were conducted to evaluate the CO_2 adsorption ability of different samples. It can be seen from Fig. 5c that the adsorption capacities of TCCN samples are superior to that of CN, implying that TCCN heterojunctions have strong abilities of CO_2 capture.[61] The CO_2 TPD profiles were recorded in a helium stream and shown in Fig. 5d. The peaks appear around 160 °C can be assigned to the desorption signal of CO_2 molecules physically adsorbed by N species of CN.[62, 63] Ti_3C_2 itself should be inactive in physical adsorbing of CO_2 without peak in this region. In contrast, TCCN heterojunctions show larger peak areas than CN, which is consistent with the results of CO_2 sorption. Besides, the desorption signals of adsorbed CO_2 appear at high temperature, attributing to the strong interaction of the basic groups.[31] These results suggest that the incorporation of Ti_3C_2 could improve the CO_2 adsorption capacities of TCCN heterojunctions.

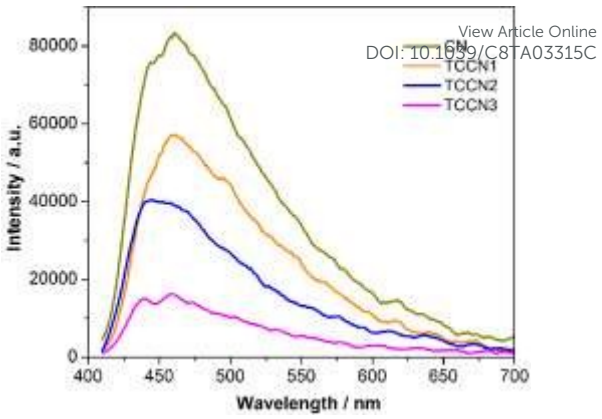

Fig. 6. PL spectra of different samples

To investigate the recombination efficiency of photo-carriers under radiation, the PL spectra of all samples were obtained under a 325 nm excitation (Fig. 6). The PL spectra evidently display an emission peak at 460 nm on account of the recombination of photo-induced electron-hole pairs. The peak intensity of TCCN heterojunction materials decreases rapidly in comparison with CN, suggesting that the recombination of electron-hole pairs is obviously suppressed.[51] As the Ti_3C_2 content increases, the peak intensity reduces gradually from TCCN1 to TCCN3, which is possibly attributed to the good transfer and utilization of charge carriers in the TCCN heterojunction.

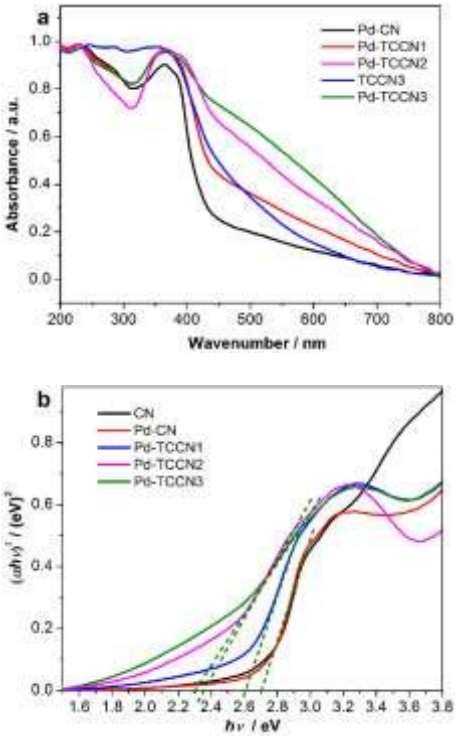

Fig. 7. (a) UV-vis absorption spectra, and (b) Tauc plots of different photocathodes

The UV−vis absorption spectra of photocathodes were displayed in Fig. 7. It can be seen that the absorption ability of TCCN3 is superior to CN due to the contribution of Ti_3C_2. After the deposition of Pd NPs, the absorption ability of Pd-TCCN3 in visible light region is

obviously improved on account of the surface plasmonic resonance of metal NPs.[64] In addition, the corresponding Tauc plots demonstrate that the band gap energies of photocathodes are 2.7 eV (Pd-CN), 2.6 eV (Pd-TCCN1), 2.36 eV (Pd-TCCN2) and 2.3 eV (Pd-TCCN3), which is favourable for light absorption and photocatalytic reactions.

3.2 Photoelectrochemical properties of photocathodes

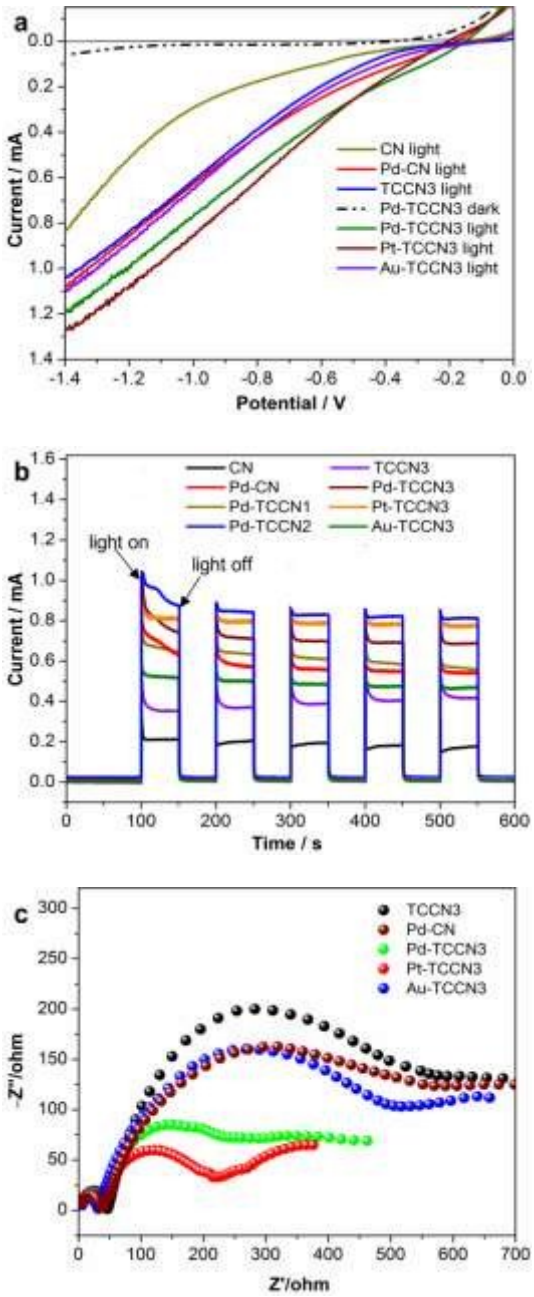

Fig. 8. (a) LSV curves, (b) transient photocurrent responses, and (c) EIS Nyquist plots of different photocathodes

The photoelectrochemical performances of photocathodes were displayed in Fig. 8 and Fig. S4. The LSV curves demonstrate that the current values of photocathodes are almost zero under the dark conditions. In contrast, the photocurrent boosts evidently with the escalation of external voltages under the light irradiation, indicating that all photocathodes have excellent photosensitivity. Furthermore, the current of Pd-TCCN photocathodes are higher than that of Pd-CN. That reveals that the formation of TCCN heterojunctions could obviously improve the efficiency of charge separation and light conversion (Fig. 8a).

The transient photocurrent responses of photocathodes were tested at −1.0 V in a two-electrode system and illustrated in Fig. 8b. When the light was turned on, the current of photocathodes raised sharply from zero to 0.7-1.0 mA. The Pd-TCCN2 gives the highest current value of 0.85 mA among the four photocathodes, which might be ascribed to the proper coupling effect of Ti_3C_2 and g-C_3N_4.

The interfacial charge transfer of photocathodes was surveyed by EIS spectra. In Nyquist plots, a smaller semicircle represents a lower resistance (R_{ct}) between the photocathode and electrolyte.[65] Obviously, the R_{ct} values of M-TCCN3 are much lower than that of TCCN3 (Fig. 8c), which could be attributed to the good transfer of charge carriers on the interface of heterojunction with the existence of metals NPs. The R_{ct} value of Pt-TCCN3 is larger than that of Pd-TCCN3 and Au-TCCN3 that was in consistent with the current data. Besides, the positive slope of Mott-Schottky plots suggests that the heterojunction is n-type semiconductor (Fig. S5). The negative flat band potential signifies that photoelectrons in conduction band of TCCN heterojunctions have a strong reducibility.[51] Furthermore, the stability of Pd-TCCN3 photocathode was examined by cyclic voltammetry (Fig. S6). After 100 cycles of continuous cyclic voltammetry, the current is slightly fluctuated, indicating that the Pd-TCCN3 photocathode is fairly stable.[66]

3.3 Photoelectrocatalytic reduction of CO_2

Initially, the PEC experiments were carried out with the two-electrode system of Pd-CN||$BiVO_4$ at an external voltage of −0.85 V (Fig. 9a). Only small amounts of $HCOO^-$ and MeOH were examined. When the Pd NPs modified TCCN heterojunctions (Pd-TCCN) were used as photocathodes, the yields of $HCOO^-$ and MeOH were speeded up evidently. Clearly, as the Ti_3C_2 content increases in TCCN heterojunction, the photocatalytic activity of photocathodes follows the order of Pd-TCCN3 > Pd-TCCN2 > Pd-TCCN1. Among all the photocathodes, Pd-TCCN3 exhibits the highest activity of CO_2 reduction to hydrocarbons in a rate of 50.2 μM cm^{-2} h^{-1} (equal to 25.1 mM h^{-1} g^{-1}) that is about tenfold of the Pd-CN. The apparent quantum efficiency of Pd-TCCN3||$BiVO_4$ cell is estimated to be 1.3 % that is two times of Pd-CN. The remarkable improvement might be attributed to the synergistic effects of pyri-N and Ti^{3+} species in TCCN3 heterojunction.

In order to investigate the influence of external voltage, the PEC experiments were carried out at various voltages using optimal Pd-TCCN3 as the photocathode. As shown in Fig. 9b, when the voltages are varied, the activity for the hydrocarbons evolution is in the order of −0.85 V > −1.05 V > −0.65 V > −0.45 V. However, the activity at −1.05 V is inferior to that of −0.85 V, because more H_2 releases at more negative voltages (Fig. S7). These results reveal that a proper voltage can accelerate the CO_2 reduction process, and contribute to the coupling of CO_2 reduction and water splitting to generate hydrocarbons. Additionally, the selectivity of liquid products was calculated and listed in Table S3. When the higher voltage was applied to the PEC cell, the higher selectivity for formic acid could be achieved in the region of −0.45 V ~ −1.05 V.

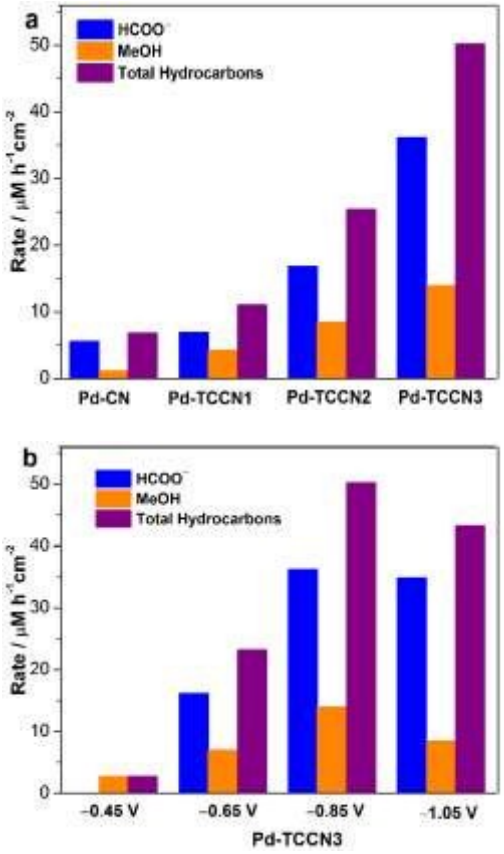

Fig. 9. The formation rate of hydrocarbons in PEC cells: (a) for four different photocathodes at −0.85 V; (b) for Pd-TCCN3 photocathode at voltages of −0.45 ~ −1.05 V in the two-electrode system

To study the influence of different metals in CO_2 reduction reaction, the M-TCCN3 electrodes were utilized as photocathodes. Even though the Pt-TCCN3 photocathode has larger current than Pd-TCCN3 in LSV curves (Fig. 8a), it produces less hydrocarbons because of more H_2 evolution (Fig. S8).[67] Therefore, Pd-TCCN3 photocathodes show higher activity in the hydrocarbons formation than that of Pt- and Au-TCCN3 due to the good matching of water splitting and CO_2 reduction (Fig. 10). These results reveal that metal Pd is more suitable for catalysis reduction of CO_2 into hydrocarbons than Pt and Au.

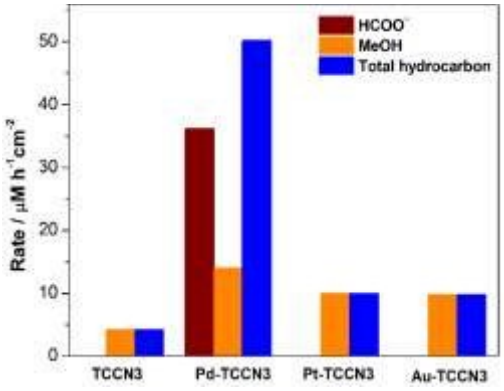

Fig. 10. The evolution rate of hydrocarbons for TCCN3 and M-TCCN3 photocathodes at −0.85 V

Furthermore, a control experiment was conducted at −0.85 V using the TCCN photocathode. As shown in Fig. 10, certain amounts of hydrocarbons and H_2 could be detected, illustrating that the heterojunction of TCCN has an eigen activity in CO_2 reduction and water splitting. Moreover, the performance of PEC cell of Pd-TCCN3||$BiVO_4$ retains in the same level after five-cycle assays (20 h), which indicates that the electrode is highly stable (Fig. S9).

3.4 $^{13}CO_2$ labelling experiments

In order to identify the carbon source of hydrocarbons, $^{13}CO_2$ labelling experiments were conducted in the same cell. The isotopic liquid products were detected by ^{1}H NMR and ^{13}C NMR spectra. As shown in Fig. 11 and S10, the doublet peak at 8.08 and 8.57 ppm is assigned to the proton of formate coupled by the ^{13}C nuclei. The distinct ^{13}C NMR signal at 160.4 ppm corresponds to the carbon of $H^{13}COO^-$ (Fig. S10).[68] These results validate that the carbon source of $HCOO^-$ is derived from CO_2.

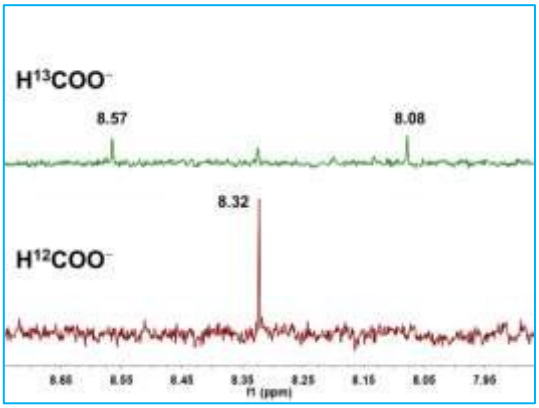

Fig. 11. ^{1}H NMR spectra of the $H^{13}COO^-$ and $H^{12}COO^-$ yielded in the PEC cell

3.5 Possible mechanism of PEC CO_2 reduction

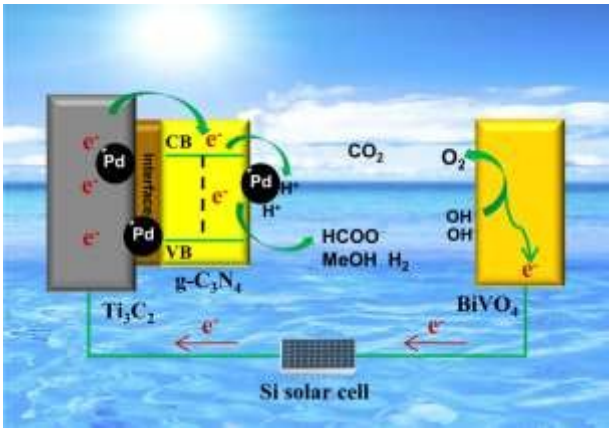

Scheme 1. A proposed mechanism for PEC reduction of CO_2 into chemical fuels

Based on the above characterizations and experimental results, a possible mechanism was proposed for PEC reduction of CO_2 into chemical fuels (Scheme 1). Initially, driven by the low external voltage, electrons could move to the Ti_3C_2 and transfer to the conduction band (CB) of g-C_3N_4 that are trapped by the protons on the surfaces of Pd NPs. Under the light irradiation, the electrons in

the valence band (VB) of g-C_3N_4 could get energy from photons and jump to the CB. Subsequently, these photoelectrons could combine with protons to generate active hydrogen atoms that directly convert CO_2 into hydrocarbons.[19, 61] In addition, the oxygen could release on the $BiVO_4$ photoanode.

Conclusions

In summary, new heterojunctions of Ti_3C_2/g-C_3N_4 were prepared and further modified by various metals, which was utilized as the photocathode in the M-TCCN||$BiVO_4$ cell to reduce CO_2. The TCCN heterojunctions have narrow band gaps and exhibit excellent ability of light harvesting. The Ti^{3+} species could suppress the recombination of photogenerated electrons and holes in heterojunctions, thereby enhancing the efficiency of photocatalysis. Besides, the Pd NPs could in-situ capture protons and pyri-N species could adsorb CO_2 molecules efficiently. These advantages of heterojunctions are favourable for the coupling of CO_2 reduction and water splitting to generate chemical fuels. To the best of our knowledge, the photoelectrocatalytic properties of Ti_3C_2/g-C_3N_4 heterojunction for CO_2 reduction have not been reported to date. This work suggests that the MXene family materials could construct heterojunction materials to store solar energy into chemical fuels via CO_2 reduction.

Conflicts of interest

There are no conflicts to declare.

Acknowledgements

This work was supported by the National Natural Science Foundation of China (NSFC 21173106), the Foundation of State Key Laboratory of Coal Conversion (J17-18-913-2), and Natural Science Foundation of Gansu Province (17JR5RA212).

Notes and references

1 C. Herrero, A. Quaranta, W. Leibl, A. W. Rutherford and A. Aukauloo, *Energy. Environ. Sci.,* 2011, **4**, 2353-2365.
2 M. Aresta, A. Dibenedetto and A. Angelini, *Chem. Rev.,* 2014, **114**, 1709-1742.
3 J. Cheng, M. Zhang, J. Liu, J. Zhou and K. Cen, *J. Mater. Chem. A,* 2015, **3**, 12947-12957.
4 X. Meng, L. Liu, S. Ouyang, H. Xu, D. Wang, N. Zhao and J. Ye, *Adv. Mater.*, 2016, **28**, 6781-6803.
5 G. Zhao, X. Huang, X. Wang and X. Wang, *J. Mater. Chem. A*, 2017, **5**, 21625-21649.
6 D. Kim, K. K. Sakimoto, D. Hong and P. Yang, *Angew. Chem. Int. Ed.,* 2015, **54**, 3259-3266.
7 J. Ronge, T. Bosserez, D. Martel, C. Nervi, L. Boarino, F. Taulelle, G. Decher, S. Bordiga and J. A. Martens, *Chem. Soc. Rev.,* 2014, **43**, 7963-7981.
8 W. Kim, E. Edri and H. Frei, *Acc. Chem. Res.,* 2016, **49**, 1634-1645.
9 S. Xie, Q. Zhang, G. Liu and Y. Wang, *Chem. Commun.*, 2016, **52**, 35-59.
10 B. Kumar, M. Llorente, J. Froehlich, T. Dang, A. Sathrum and C. P. Kubiak, *Annu. Rev. Phy.s Chem.*, 2012, **63**, 541-569.
11 X. Li, J. Wen, J. Low, Y. Fang and J. Yu, *Sci. China Mater.*, 2014, **57**, 70-100.
12 P. Wang, S. Wang, H. Wang, Z. Wu and L. Wang, *Part. Part. Syst. Char.*, 2018, **35**, 1700371.
13 G. Magesh, E. S. Kim, H. J. Kang, M. Banu, J. Y. Kim, J. H. Kim and J. S. Lee, *J. Mater. Chem. A*, 2014, **2**, 2044-2049.
14 X. Chang, T. Wang and J. Gong, *Energy. Environ. Sci.,* 2016, **9**, 2177-2196.
15 J. L. White, M. F. Baruch, J. E. Pander Iii, Y. Hu, I. C. Fortmeyer, J. E. Park, T. Zhang, K. Liao, J. Gu, Y. Yan, T. W. Shaw, E. Abelev and A. B. Bocarsly, *Chem. Rev.*, 2015, **115**, 12888-12935.
16 K. Sivula and R. van de Krol, *Nat. Rev. Mater.,* 2016, **1**, 15010.
17 B. Weng, W. Wei, Y. Yiliguma, H. Wu, A. M. Alenizi and G. Zheng, *J. Mater. Chem. A*, 2016, **4**, 15353-15360.
18 W. Lu, B. Jia, B. Cui, Y. Zhang, K. Yao, Y. Zhao and J. Wang, *Angew Chem. Int. Ed.,* 2017, **56**, 11851-11854.
19 Y. Xu, Y. Jia, Y. Zhang, R. Nie, Z. Zhu, J. Wang and H. Jing, *Appl. Catal. B*, 2017, **205**, 254-261.
20 W. J. Ong, L. L. Tan, Y. H. Ng, S. T. Yong and S. P. Chai, *Chem. Rev.,* 2016, **116**, 7159-7329.
21 X. Wang, K. Maeda, A. Thomas, K. Takanabe, G. Xin, J. M. Carlsson, K. Domen and M. Antonietti, *Nat. Mater.*, 2009, **8**, 76-80.
22 X. Wang, X. Chen, A. Thomas, X. Fu and M. Antonietti, *Adv. Mater.*, 2009, **21**, 1609-1612.
23 Y. Wang, X. Wang and M. Antonietti, *Angew. Chem. Int. Ed.,* 2012, **51**, 68-89.
24 R. Kuriki, H. Matsunaga, T. Nakashima, K. Wada, A. Yamakata, O. Ishitani and K. Maeda, *J. Am. Chem. Soc.,* 2016, **138**, 5159-5170.
25 M. Shalom, S. Inal, C. Fettkenhauer, D. Neher and M. Antonietti, *J. Am. Chem. Soc.*, 2013, **135**, 7118-7121.
26 S. Ye, R. Wang, M. Wu and Y. Yuan, *Appl. Surf. Sci.*, 2015, **358**, 15-27.
27 S. Tonda, S. Kumar, S. Kandula and V. Shanker, *J. Mater. Chem. A*, 2014, **2**, 6772-6780.
28 N. Sagara, S. Kamimura, T. Tsubota and T. Ohno, *Appl. Catal. B*, 2016, **192**, 193-198.
29 W. Yu, D. Xu and T. Peng, *J. Mater. Chem. A*, 2015, **3**, 19936-19947.
30 C. Liu, H. Huang, L. Ye, S. Yu, N. Tian, X. Du, T. Zhang and Y. Zhang, *Nano Energy*, 2017, **41**, 738-748.
31 J. Liu, H. Shi, Q. Shen, C. Guo and G. Zhao, *Green. Chem.*, 2017, **19**, 5900-5910.
32 C. Yu, H. Fang, Z. Liu, H. Hu, X. Meng and J. Qiu, *Nano Energy*, 2016, **25**, 184-192.
33 J. Zhang, G. Zhang, X. Chen, S. Lin, L. Mohlmann, G. Dolega, G. Lipner, M. Antonietti, S. Blechert and X. Wang, *Angew. Chem. Int. Ed.*, 2012, **51**, 3183-3187.
34 L. Yang, J. Huang, L. Shi, L. Cao, H. Liu, Y. Liu, Y. Li, H. Song, Y. Jie and J. Ye, *Appl. Catal. B*, 2018, **221**, 670-680.
35 F. Li, M. Xue, J. Li, X. Ma, L. Chen, X. Zhang, D. R. MacFarlane and J. Zhang, *Angew. Chem. Int. Ed.,* 2017, **56**, 14718-14722.
36 T. Ma, J. Cao, M. Jaroniec and S. Qiao, *Angew. Chem. Int. Ed.*, 2016, **55**, 1138-1142.
37 W. Yu, D. Xu, and T. Peng, *J. Mater. Chem. A,* 2015, **3**, 19936-19947.
38 J. Fu, B. Zhu, C. Jiang, B. Cheng, W. You, and J. Yu, *Small,* 2017, **13**, 1603938.
39 B. Anasori, M. R. Lukatskaya and Y. Gogotsi, *Nat. Rev. Mater.,* 2017, 2, 16098.
40 V. M. Hong Ng, H. Huang, K. Zhou, P. S. Lee, W. Que, J. Z. Xu and L. B. Kong, *J. Mater. Chem. A*, 2017, **5**, 3039-3068.

View Article Online
DOI: 10.1039/C8TA03315C

41 O. Mashtalir, K. M. Cook, V. N. Mochalin, M. Crowe, M. W. Barsoum and Y. Gogotsi, *J. Mater. Chem. A,* 2014, **2**, 14334-14338.
42 M. Naguib, V. N. Mochalin, M. W. Barsoum and Y. Gogotsi, *Adv. Mater.,* 2014, **26**, 992-1005.
43 H. Zhang, G. Yang, X. Zuo, H. Tang, Q. Yang and G. Li, *J. Mater. Chem. A*, 2016, **4**, 12913-12920.
44 C. Peng, X. F. Yang, Y. H. Li, H. Yu, H. J. Wang and F. Peng, *ACS Appl. Mater. Interfaces,* 2016, **8**, 6051-6060.
45 J. Ran, G. Gao, F. Li, T. Ma, A. Du and S. Qiao, *Nat. Commun.*, 2017, **8**, 13907.
46 X. Zhang, Z. H. Zhang, J. L. Li, X. D. Zhao, D. H. Wu, Z. Zou, *J. Mater. Chem. A*, 2017, **5**, 12899-12903.
47. S. Wang, J. Ma, S. Zhu, J. Cheng, Z. Qiao, J. Yang, W. Liu, *Mater. Des.,* 2015, **67**, 188-196.
48. M. Naguib, M. Kurtoglu, V. Presser, J. Lu, J. J. Niu, M. Heon, L. Hultman, Y. Gogotsi, M. W. Barsoum, *Adv. Mater.*, 2011, **23**, 4248-4253.
49. M. Ghidiu, M. R. Lukatskaya, M. Q. Zhao, Y. Gogotsi, M. W. Barsoum, *Nature*, 2014, **516**, 78-U171.
50 Y. Jia, Y. Xu, R. Nie, F. Chen, Z. Zhu, J. Wang and H. Jing, *J. Mater. Chem. A*, 2017, **5**, 5495-5501.
51 C. Yang, J. Qin, Z. Xue, M. Ma, X. Zhang and R. Liu, *Nano Energy,* 2017, **41**, 1-9.
52. X. Zou, G. Li, Y. Wang, J. Zhang, C. Yan, M. Guo, L. Li, J. Chen, *Chem. Commun.*, 2011, **47**, 1066-1068.
53 I. S. Amiinu, X. Liu, Z. Pu, W. Li, Q. Li, J. Zhang, H. Tang, H. Zhang and S. Mu, *Adv. Funct. Mater.*, 2017, **5**, 1704638.
54 Q. Li, R. Cao, J. Cho, and G. Wu, *Adv. Energy. Mater.*, 2014, **4**, 1301415.
55 Y. Zhu, Z. Xu, W. Jiang, S. Zhong, L. Zhao and S. Bai, *J. Mater. Chem. A*, 2017, **5**, 2619-2628.
56 K. Li, S. Gao, Q. Wang, H. Xu, Z. Wang, B. Huang, Y. Dai and J. Lu, *ACS Appl. Mater. Interfaces*, 2015, **7**, 9023-9030.
57 G. Li, J. Li, G. Li and G. Jiang, *J. Mater. Chem. A*, 2015, **3**, 22073-22080.
58 X. Liu, S. Gao, H. Xu, Z. Lou, W. Wang, B. Huang and Y. Dai, *Nanoscale*, 2013, **5**, 1870-1875.
59 J. Zhang, M. Zhang, G. Zhang and X. Wang, *ACS Catal.*, 2012, **2**, 940-948.
60 Y. Xu, S. Wang, J. Yang, B. Han, R. Nie, J. Wang, J. Wang, H. Jing, *Nano Energy,* 10.1016/j.nanoen.2018.06.086.
61 A. Crake, K. C. Christoforidis, A. Kafizas, S. Zafeiratos, C. Petit, *Appl. Catal. B*, 2017, **210**, 131-140.
62 S. N. Talapaneni, S. Anandan, G. P. Mane, C. Anand, D. S. Dhawale, S. Varghese, A. Mano, T. Mori, A. Vinu, *J. Mater. Chem.,* 2012, **22**, 9831-9840.
63 N. Li, X. Zou, M. Liu, L. Wei, Q. Shen, R. Bibi, C. Xu, Q. Ma, J. Zhou, *J. Phys. Chem. C*, 2017, **121**, 25795-25804.
64 W. Hou and S. B. Cronin, *Adv. Funct. Mater.*, 2013, **23**, 1612-1619.
65 F. Gou, X. Jiang, R. Fang, H. Jing and Z. Zhu, *ACS Appl. Mater. Interfaces*, 2014, **6**, 6697-6703.
66 X. Huang, Q. Shen, J. Liu, N. Yang and G. Zhao, Energy & Environ. *Sci.*, 2016, **9**, 3161-3171.
67 T. Tong, B. Zhu, C. Jiang, B. Cheng, J. Yu, *Appl. Surf. Sci.,* 2018, **433**, 1175-1183.
68 S. Gao, Y. Lin, X. Jiao, Y. Sun, Q. Luo, W. Zhang, D. Li, J. Yang and Y. Xie, *Nature*, 2016, **529**, 68-71.

View Article Online
DOI: 10.1039/C8TA03315C

Graphical abstract

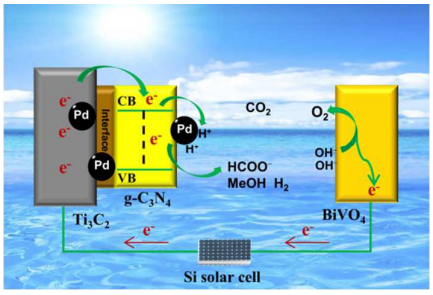

The new heterojunction of Ti_3C_2/g-C_3N_4 with rich Ti^{3+} and pyri-N species could efficiently photoelectrocatalytic convert CO_2 into hydrocarbons.